Applied Ocean Research 154 (2025) 104392

Contents lists available at ScienceDirect

Applied Ocean Research

journal homepage: www.elsevier.com/locate/apor

Research paper

Experimental study on the effect of an underground structure on the seismic responses of saturated coral sand site

Zhongxiang Zhang [a], Su Chen [a,*], Yongzhi Wang [c], Xiaojun Li [a,b]

[a] State Key Laboratory of Bridge Safety and Resilience, Beijing University of Technology, Beijing 100124, China
[b] Institute of Geophysics, China Earthquake Administration, Beijing 100081, China
[c] Institute of Engineering Mechanics, China Earthquake Administration, Harbin 150080, China

ARTICLE INFO

Keywords:
Coral sand
Underground structure
Centrifuge shaking table tests
Seismic response
Liquefaction
Soil-structure interaction

ABSTRACT

Understanding the effect of underground structures on the seismic responses of saturated coral sand sites is crucial for improving seismic design and preventing liquefaction disasters in island reef engineering. Despite advancements in this field, the specific effects of underground structures on the seismic behavior of coral sand sites remain underexplored. This study addresses this issue by conducting dynamic centrifuge shaking table tests on saturated coral sand sites, both with and without an underground structure. The seismic responses between the free field (FF) and structure field (SF) were compared in terms of pore pressure, acceleration, response spectra, and shear stress-strain behavior. Test results reveal that the presence of the underground structure led to a deeper liquefaction zone beneath it. The excess pore pressure in the soil layer above the structure dissipated rapidly after peaking and completely dissipated by the end of the seismic motions. Additionally, the soil near the bottom of the structure exhibited higher dilatancy. The structure amplified the acceleration of the soil above and near its bottom while reducing the acceleration of the soil adjacent to its sidewall. In the period range of 0.9–3.0 s, the presence of the structure weakened the attenuation of response spectra values for the soil adjacent to the sidewall and above the structure. Furthermore, the structure limited the deformation of the soil adjacent to its sidewall and increased the soil shear modulus.

1. Introduction

With the development of marine resources, the construction of island reef engineering has been accelerating. Coral sand, utilized as a foundational filling material, is extensively employed in reclamation projects in coral reef regions. There are significant differences in the mechanical properties between coral sand and siliceous sand (Wu et al., 2020; Xiao et al., 2017). Compared to siliceous sand, coral sand exhibits higher dynamic cyclic strength, greater shear stiffness, and a lower damping ratio (Ding et al., 2021; Ha Giang et al., 2017; Javdanian and Jafarian, 2018; Liu et al., 2020). In addition, coral sand has a higher resistance to liquefaction (Chen et al., 2024; Liu et al., 2021; Ma et al., 2021). The regions where coral reefs are located are susceptible to significant seismic risks. Previous studies have reported severe seismic disaster events at coral sand sites. Lateral spreading and uneven subsidence caused by liquefaction at coral sand sites led to significant structural damage during the 1993 Guam earthquake (Mejia and Yeung, 1995). Severe port damage and underground pipeline destruction were observed due to the liquefaction of the coral sand foundation during the 2006 Hawaii earthquake and the 2010 Haiti earthquake (Chock et al., 2006; Olson et al., 2011).

Considering the shortage of land resources on island reefs, it is extremely essential to develop underground spaces. Therefore, the seismic responses of underground structures at coral sand sites have attracted widespread attention. Wu et al. (2020) compared the seismic response of pile group foundations in coral sand and Fujian sand through shaking table tests. They found that the pile bending moment in coral sand was smaller than that in Fujian sand. Ding et al. (2021) investigated the seismic responses of underground structures in coral sand under different groundwater levels. The results reveal that the acceleration amplification factor, dynamic strain, and bending moment of underground structures at coral sand sites decreased with the increase of the groundwater level. The coral sand-pile-superstructure dynamic interaction was explored by numerical simulation. The results show that the pile bending moment reduced with the decrease in the permeability of the coral sand (Wu et al., 2023a). Wu et al. (2023b) established coral

* Corresponding author.
E-mail address: chensuchina@126.com (S. Chen).

https://doi.org/10.1016/j.apor.2024.104392
Received 14 September 2024; Received in revised form 20 November 2024; Accepted 23 December 2024

sand-structure numerical models in FLAC3D and concluded that an increase in the relative density of coral sand would cause higher horizontal dynamic earth pressure on the underground structure. Soil liquefaction could increase the energy dissipation of the coral sand-underground structure system (Wu et al., 2024).

However, the above research primarily focused on the seismic response of underground structures in the context of soil-structure interaction in coral sand, with few studies concerning the effect of underground structures on the seismic behaviors of saturated coral sand sites. Moghadam and Baziar (2016) studied surface acceleration in a subway tunnel site. This study indicated that spectral acceleration shifted toward longer periods as the tunnel flexibility ratio increased. Sun et al. (2019) investigated the influence of subway stations on the surface ground motion under vertical seismic motions, and significant peak shear strain amplification was observed at the top of the station. Mashhadban et al. (2021) declared that the presence of a horseshoe tunnel influenced the dynamic behavior of slopes and seismic motions of the inclined surface of the slope were amplified. Wang et al. (2018) conducted a shaking table model test on an underground structure-soil-surface structure interaction system. The results demonstrate that the presence of the tunnel hindered the propagation of seismic motion and reduced the peak ground acceleration of the ground surface. This is consistent with the findings by Baziar et al. (2014) and Abuhajar et al. (2015). In contrast, obvious amplification of the ground motions was observed in other studies (Besharat et al., 2012; Feizi et al., 2022; Isari et al., 2022; Tsinidis et al., 2014). Dou et al. (2022) conducted two groups of shaking table tests to explore the effect of pile-supported structures on the saturated siliceous sand site. They found that the existence of structures increased the liquefaction resistance of the site. Therefore, it is crucial to explore the effect of the underground structure on the dynamic responses of coral sand sites, which could aid in seismic design and liquefaction disaster prevention for island reef engineering.

This paper compared the results of centrifuge shaking table tests on a saturated coral sand site with and without an underground structure. The influences of the underground structure on the seismic responses of the site, including the pore pressure, acceleration, response spectra, and shear stress-strain behavior, were analyzed in detail.

2. Experimental setup

2.1. Testing equipment

The experiments were conducted on a 300 g-t centrifuge at the Institute of Engineering Mechanics, China Earthquake Administration. The centrifuge has an effective radius of 5 m and a centrifugal acceleration of 50 g. A unidirectional shaking table installed on the centrifuge can simulate complex seismic motions with a maximum amplitude of 30 g and a frequency range of 10–300 Hz. More specific experimental equipment parameters can be found in previous research (Zhang et al., 2024). The test models were prepared in a rigid container with a steel partition plate in the middle. The internal dimensions of the container are 78 cm (length) × 58 cm (width) × 60 cm (height) and 52 cm (length) × 58 cm (width) × 60 cm (height) in model scale. To mitigate the potential boundary effect, a 4 cm thick polystyrene foam board was affixed to the inner walls of the container in a direction perpendicular to the shaking. The experiments were conducted under a centrifugal acceleration of 50 g and the scale factors are listed in Table 1 (Kutter, 1992). All the results discussed subsequently were on the prototype scale.

2.2. Test material

The coral sand employed in this study was derived from the reclaimed land of a certain island reef. The grain size distribution curve of the sand is presented in Fig. 1, obtained by the previous studies (Gao and Ye, 2023; Wu et al., 2023). The basic properties of the sand are listed in Table 2.

Table 1
The scale factors for dynamic centrifuge tests.

Physical quantity	Dimensions	Model/Prototype
Length	L	1/50
Density	ML^{-3}	1
Elastic modulus	$ML^{-1}T^{-2}$	1
Stress	$ML^{-1}T^{-2}$	1
Strain	—	1
Acceleration	LT^{-2}	50
Velocity	LT^{-1}	1
Displacement	L	1/50
Time (dynamic)	T	1/50
Time (consolidation)	T	$1/50^2$
Frequency	T^{-1}	50

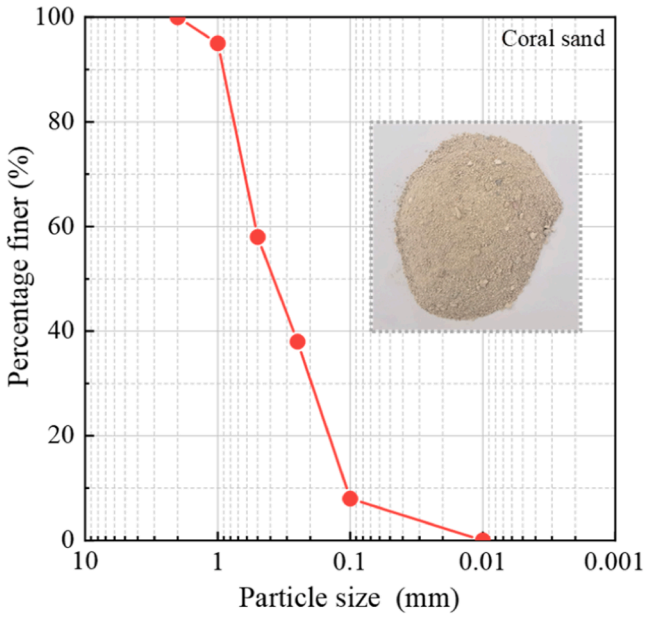

Fig. 1. The grain size distribution curve.

The underground structure model was constructed using an aluminum alloy material with a density of 2.8 × 10^3 kg/m^3, which is comparable to the density of reinforced concrete (Yatsumoto et al., 2019; Jafarian et al., 2021; Zhang et al., 2021; Zhu et al., 2021; Wang et al., 2022). Fig. 2(c) displays the structure model, with dimensions of 150 mm width, 100 mm height, and 15 mm thickness. The end of the model structure was sealed with a 3 mm thick acrylic sheet, which was bonded using epoxy resin and further sealed with waterproof tape. This setup effectively prevented water and sand from entering the model structure.

2.3. Designation of the model and instrumentation

Wang et al. (2021) reported that the geological structure of the island reef as comprising two layers: an upper layer of coral sand about 17 m thick and a lower reef limestone layer. Thus, the test models were divided into two layers. Due to the similarity of compressive strength,

Table 2
Basic properties of the coral sand.

D_r	D_{10} (mm)	D_{50} (mm)	C_u	C_c	Minimum dry density ρ_{min}(g/cm^3)	Maximum dry density ρ_{max}(g/cm^3)
50%	0.110	0.400	5	1	1.312	1.709

elastic modulus, and density between C15 concrete and reef limestone (Wang, 2008), a C15 concrete slab was used to simulate the reef limestone layer. As shown in Fig. 2(a), the left side of the rigid container was configured as the structure field model, while the right side is the free field model. This can ensure consistent seismic inputs between the structure field and the free field. The underground structure was buried at a depth of 1.5 m on a prototype scale.

Fig. 2(a) and (b) present the soil profile and sensor layout of the test models. Various transducers were employed in both models to measure the acceleration, pore pressure, and displacement of the soil surface and the underground structure. The acceleration transducers are represented in the figures by the letter A. A0 was installed on the model container to record the seismic input motions. For the structure field model, A1-A3 were used to measure the acceleration of the soil away from the base of the structure. A4-A6, A12, and A13 were installed around the underground structure to record the acceleration of the soil surrounding the structure. A7-A11 were installed to monitor the boundary effect. A14 was used to record the acceleration of the structure. The pore pressure transducers are shown by the letter P in the figures. P0-P2, P12, and P13 were employed to measure the pore pressure in the soil away from the base of the structure. P3-P5, P10, and P11 were installed to monitor the pore pressure in the soil surrounding the structure. The linear variable differential transformers are represented in the figures by the letter L. L1 and L2 were used to measure the displacement of the structure and the soil surface, respectively. All the transducers with the same labels in the free field were installed at the same depths as those in the structure field.

2.4. Model preparation and test cases

To maintain model uniformity, the coral sand layer was divided into several sublayers. Each sublayer was prepared according to the grain size distribution curves. The coral sand with a relative density of 50%

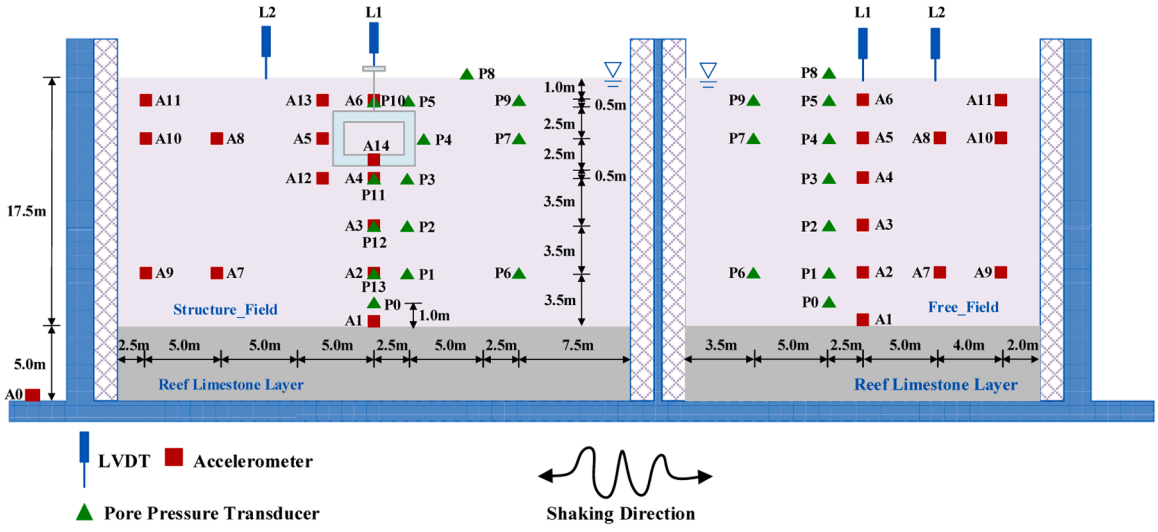

(a) Soil profile

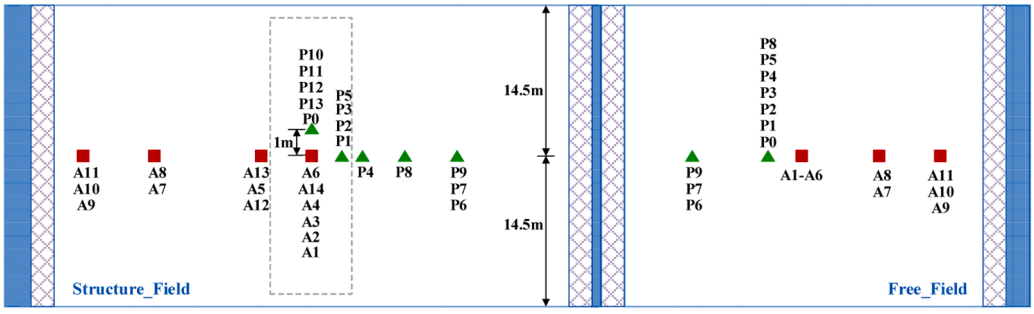

(b) Top view

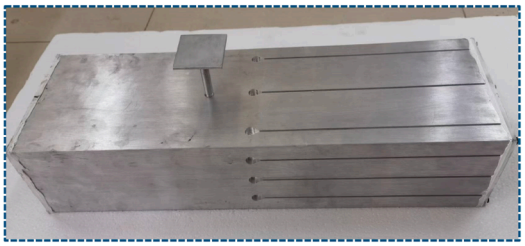

(c) Structure model

Fig. 2. Soil profile and sensor layout.

was achieved by controlling the mass of each sublayer to be equal to the theoretical value. The methylcellulose solution with a viscosity of 50 cSt was employed as the pore fluid to resolve the disagreement between the time scale factor for dynamic and consolidation at a centrifuge acceleration of 50 g (Adamidis and Madabhushi, 2015). Then, the models were placed in a vacuum device to saturate. The detailed saturation process was comprehensively described in previous research (Zhang et al., 2024).

Fig. 3 displays the acceleration time histories and Fourier spectra of the 0.1 g input motions recorded by A0. The Motion1 was recorded by the K-net submarine station KNG204 during the 2011 Great East Japan earthquake, and the Motion2 was recorded by station KNG205 during the 2006 East Coast of Izu Peninsula earthquake. It is noted that there are significant differences between Motion1 and Motion2. The Motion1 has abundant low-frequency components and long duration.

To investigate the differences in the seismic response between the free field and structure field under the various intensities of ground motions. The acceleration amplitudes of the two seismic motions were scaled to 0.1 g, 0.2 g, and 0.3 g, respectively. The input motion sequence is listed in Table 3.

Table 3
The input motion sequence.

Shake sequence	Input motion type	Amplitude (g)
1	Motion1	0.10
2	Motion2	0.10
3	Motion1	0.20
4	Motion2	0.20
5	Motion1	0.30
6	Motion2	0.30

3. Result and discussion

3.1. Effect of the underground structure on pore pressure response

The effect of the underground structure on pore pressure development of site soil was investigated by comparing the results of the free field (FF) and structure field (SF). Fig. 4 shows the maximum values of the excess pore pressure ratio ($r_{u,\ max}$) beneath the structure. In Fig. 4, the first and second columns present the $r_{u,\ max}$ under the Motion1 and Motion2, respectively. The $r_{u,\ max}$ values exceeding 1 could be attributed to a momentary increase in total vertical stresses. This increase might result from dynamic vertical accelerations caused by container rocking during horizontal shaking, or from pulling and pushing on sensor cables due to soil movement or interaction between the soil and sensors (Hughes and Madabhushi, 2018; Kutter et al., 2020; Manandhar et al., 2021). There was a significant discrepancy in the pore pressure response beneath the structure between the FF and SF. Due to the existence of the underground structure, the $r_{u,\ max}$ at different depths in the SF was higher than that in the FF. It could be attributed to the underground structure blocking the direct migration of pore water from the deep to the shallow layer and prolonging the drainage path. Under 0.1 g ground motions, the difference in the $r_{u,\ max}$ between the two sites gradually decreased as the distance from the structure increased. However, this phenomenon was not obvious with the increase in the intensity of shaking, indicating that the influence depth of underground structure on the development of pore pressure increased with the increase of ground motion intensity. In addition, liquefaction occurred under 0.2 g and 0.3

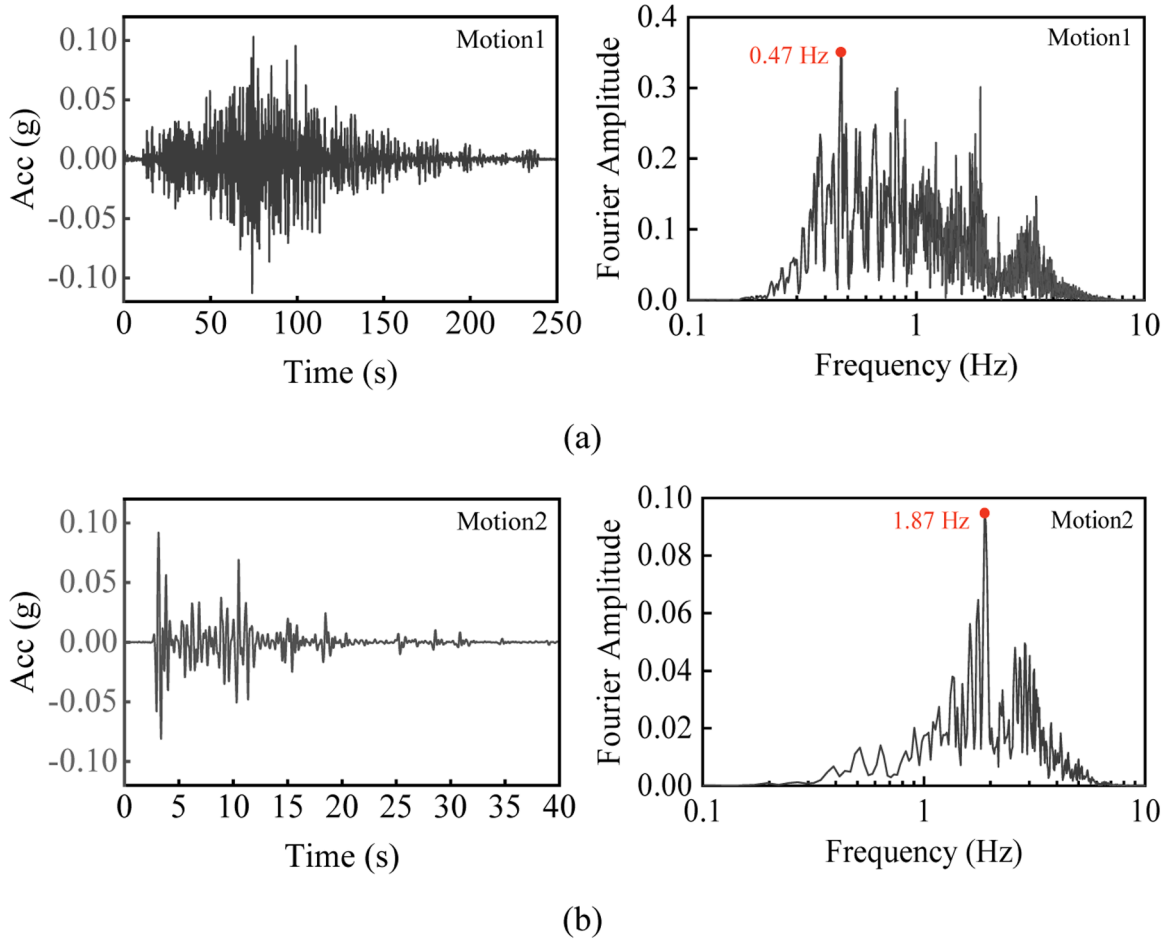

Fig. 3. The acceleration time histories and Fourier spectra of the 0.1 g input motions: (a) Motion1, (b) Motion2.

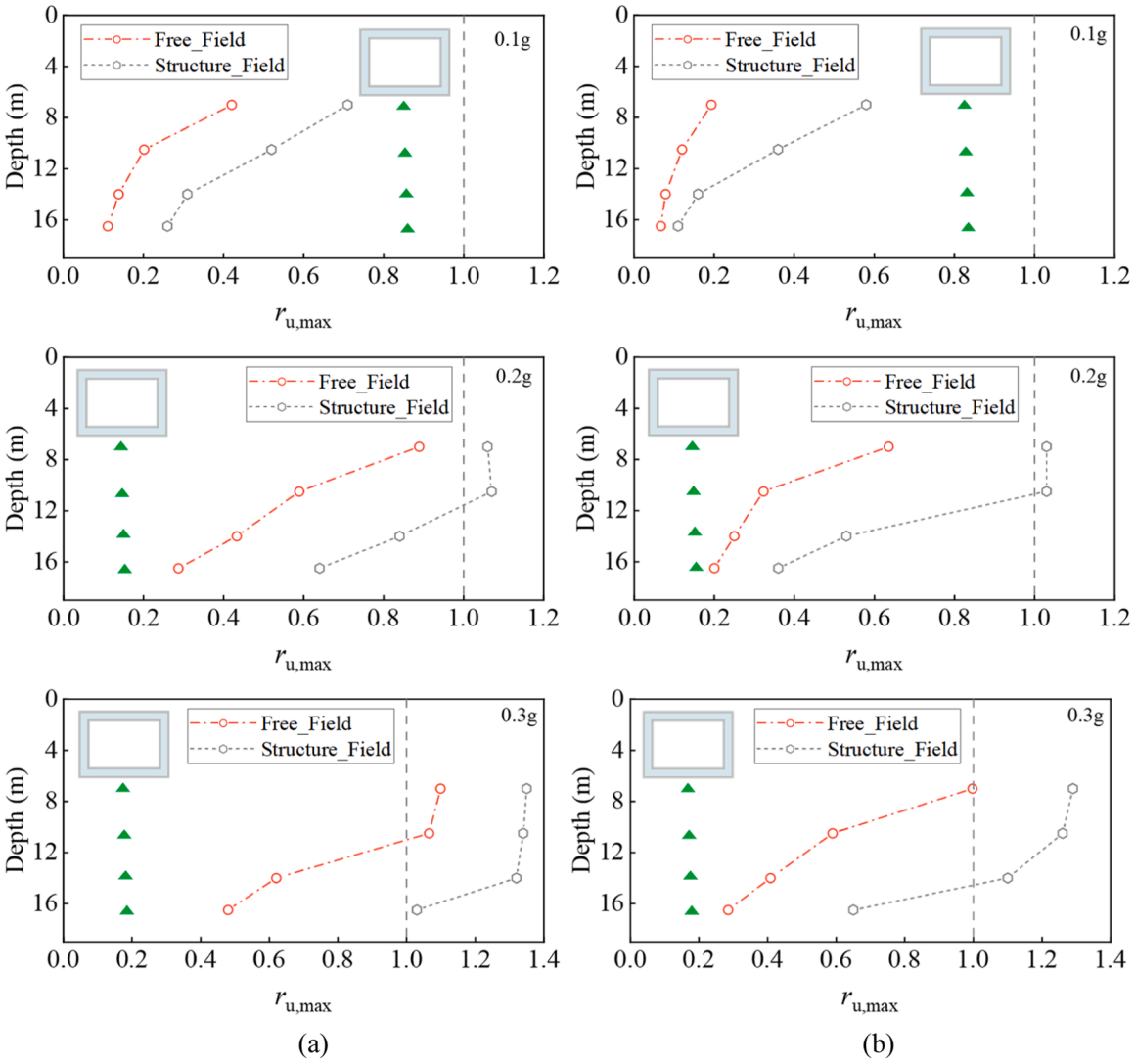

Fig. 4. The $r_{u,\ max}$ beneath the structure under different seismic motions: (a) Motion1, (b) Motion2.

g seismic motions, and the liquefaction depth in the SF was greater than that in the FF. It could be concluded that the presence of the underground structure would increase the liquefaction depth of the soil beneath the structure.

Three pore pressure transducers were used to monitor the influence of the structure on the pore pressure response of the surrounding soil. Results were similar between 0.2 g and 0.3 g shaking events and therefore only the results for 0.2 g input motions are presented. Fig. 5 displays the time histories of r_u at P11 in the FF and SF under different input motions. The results in Fig. 5 clearly show that the excess pore pressure was larger in the SF. This is because the existence of the structure changed the dissipation path of the excess pore water and hindered the migration of the pore water. Additionally, it is noted that a large number of dilation spikes were observed during the pore pressure development in the SF under various motions, signifying higher dilatancy. It could be concluded that soil-structure interaction had a significant influence on the dilatancy characteristics of the soil layer near the bottom of the structure.

Fig. 6 shows the time histories of excess pore pressure ratios (r_u) at P4 in the FF and SF under different input motions. As shown in Fig. 6(a) and (c), the r_u at P4 in the SF was larger than that in the FF and liquefaction occurred at P4 in the SF under 0.1 g Motion1, indicating that the structure increased excess pore pressure in the soil adjacent to its sidewall. However, in the dissipation stage of excess pore pressure, the dissipation velocity in the SF was greater than that in the FF. As can be noted from Fig. 6(b) and (d), for the 0.2 g seismic motions, the dissipation of excess pore pressure at P4 in the SF occurred earlier than that in the FF when the soil layer reached a liquefaction state. There is one possible explanation for this. The contact area between the side wall of the underground structure and the soil formed a drainage channel under the seismic motions, which accelerated the dissipation of excess pore pressure in the SF. A similar observation was reported by other researchers (Dou et al., 2022).

The comparisons for pore pressure development in the soil layer above the underground structure between the FF and SF are shown in Fig. 7. Results were similar from all of the seismic motions and therefore only the results for 0.1 g Motion1 and Motion2 are presented in the figure. The time histories of r_u at P10 exhibited obvious differences between the FF and SF. The rapid accumulation of excess pore pressure in the FF began earlier than in the SF under the Motion1. The r_u in the FF was greater than that in the SF and the soil layer above the structure was close to liquefaction in the FF under the same shaking. The excess pore pressure dissipated rapidly after reaching its peak in the SF. In addition, the excess pore pressure in the SF had completely dissipated at the end of the shaking, while it had not begun to dissipate in the FF. For the FF, it can be attributed to the upward migration of pore fluid from the bottom layers, increasing the severity of liquefaction. However, for the SF, the underground structure blocked the continuing upward migration of pore

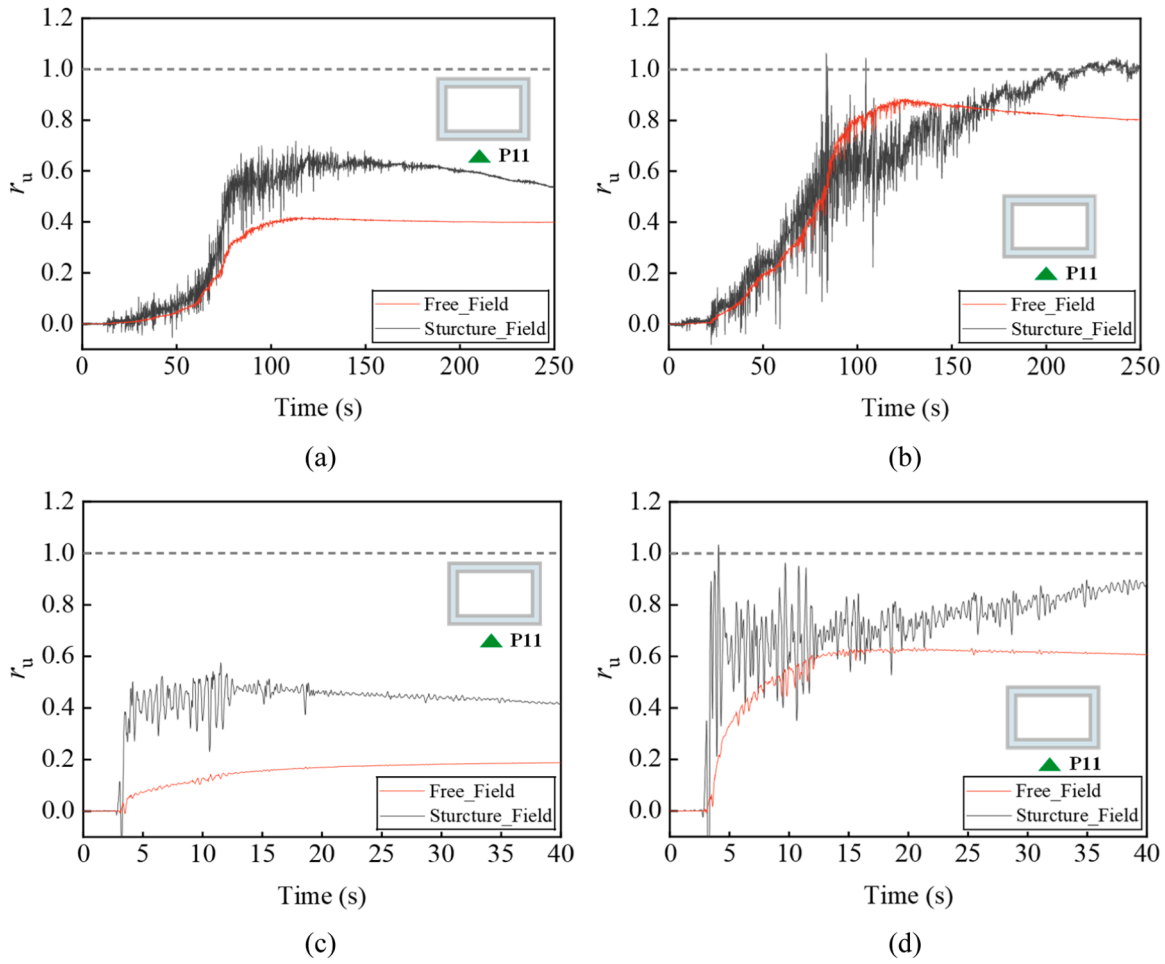

Fig. 5. Time histories of excess pore pressure ratios (r_u) at P11 in the FF and SF: (a) 0.1 g Motion1, (b) 0.2 g Motion1, (c) 0.1 g Motion2 and (d) 0.2 g Motion2.

fluid from the deep to the shallow layer, ensuring the rapid dissipation of the excess pore pressure in the soil layer above the structure.

3.2. Effect of the underground structure on acceleration response

3.2.1. Arias intensity

The Arias intensity I_a represents the total seismic energy, which integrates the amplitude, frequency, and duration of ground motion (Arias A, 1970). The Arias intensity I_a can be obtained by the Eq. (1).

$$I_a = \frac{\pi}{2g}\int_0^{T_d} a(t)^2 dt \tag{1}$$

where a(t) is the time history of the acceleration, T_d is the duration of the acceleration, and g is the gravitational acceleration. The Arias intensity amplification factor (AAF) at each accelerometer depth is the ratio between the Arias intensity of soil acceleration and the base input motion as stated in Eq. (2).

$$AAF = \frac{I_a(\mathrm{A1}-\mathrm{A3})}{I_a(\mathrm{A0})} \tag{2}$$

The AAF can be used to investigate the differences in the propagation law of seismic motions beneath the structure between the FF and SF. The effect of the structure on the Arias intensity around the structure was analyzed in detail in the next section. In Fig. 8, the first and second columns present the AAF beneath the structure (A1-A3) under the Motion1 and Motion2, respectively. There was obvious seismic energy amplification at the two sites, and the AAF at A3 in the FF was greater than that in the SF. As the distance from the structure decreased, the difference in AAF between the two sites gradually increased, indicating the influence of the structure on the seismic wave propagation. In addition, as the intensity of seismic motion increased, the difference in AAF between the two sites gradually increased, and the AAF at various depths in the FF was larger than that in the SF. The presence of the underground structure restricted the propagation of seismic energy. As mentioned earlier, the structure increased excess pore pressure in the soil beneath the structure. It caused more severe soil softening and stiffness loss, increased soil damping, and weakened the upward propagation of shear wave energy.

3.2.2. Acceleration time histories

To investigate the effect of the underground structure on the acceleration response in the soil around the structure, the acceleration time histories above, on the side, and below the structure in the FF and SF were compared. Results were similar from all of the seismic motions and therefore only the results for 0.1 g Motion1 and Motion2 are presented. The comparison of corresponding Arias intensity was also shown.

Fig. 9 displays the acceleration time histories and Arias intensity at A4 at the two sites. For the Motion1, the results show that the peak ground acceleration (PGA) and seismic energy in the FF were smaller compared to the SF. For the Motion2, although the PGA in the SF and FF was close, the seismic energy at A4 in the SF was greater than that in the FF. This phenomenon was also observed in a previous study (Wang et al., 2022). This indicates that the existence of the underground structure would increase the seismic motions of the soil layer near the bottom the structure. As shown in Fig. 5, the excess pore pressure at A4 in the SF was much greater than that in the FF, signifying more severe soil softening

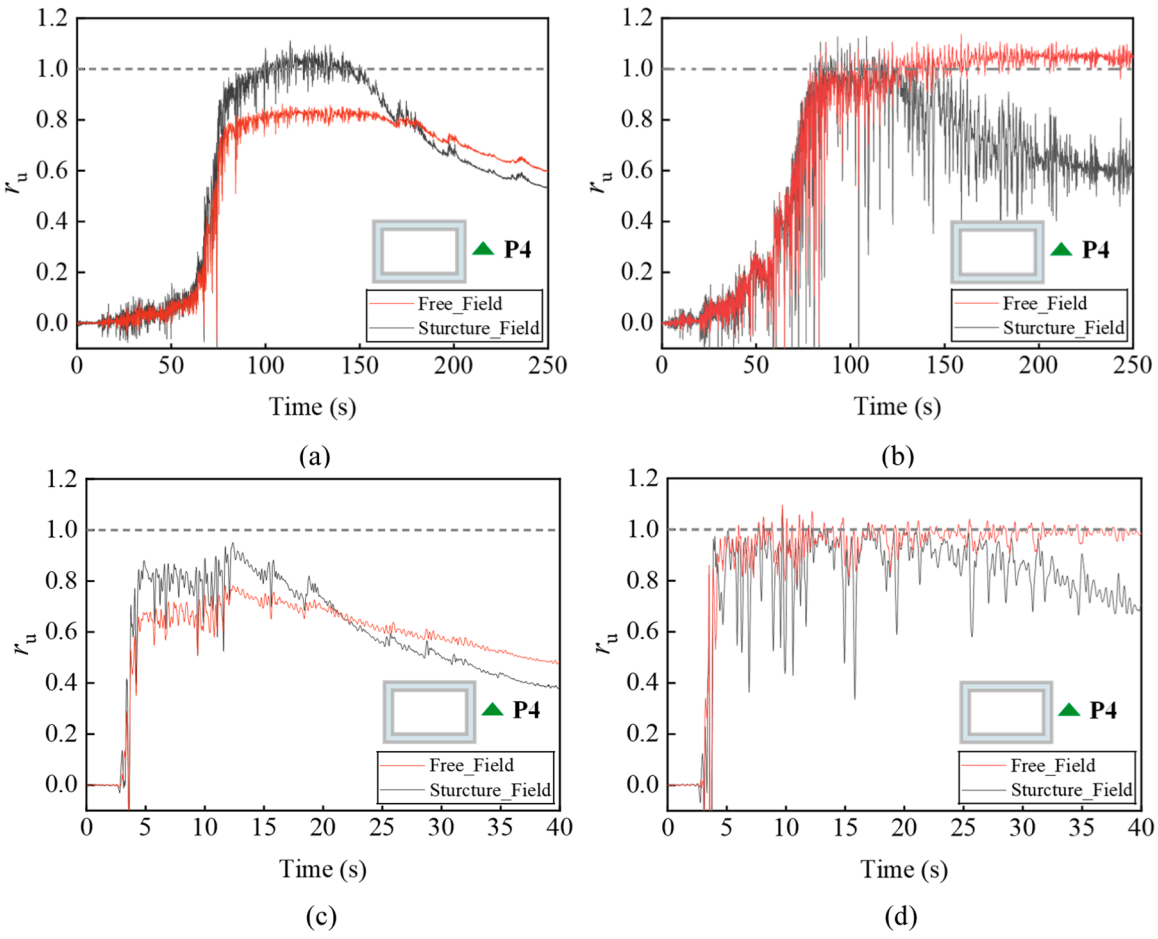

Fig. 6. Time histories of excess pore pressure ratios (r_u) at P4 in the FF and SF: (a) 0.1 g Motion1, (b) 0.2 g Motion1, (c) 0.1 g Motion2 and (d) 0.2 g Motion2.

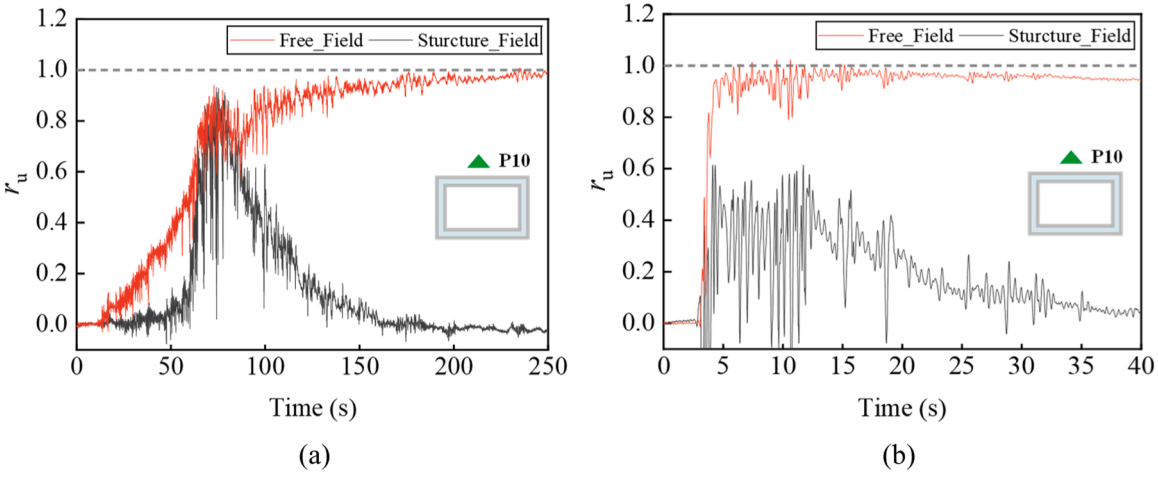

Fig. 7. Time histories of excess pore pressure ratios (r_u) at P10 in the FF and SF: (a) 0.1 g Motion1, (b) 0.1 g Motion2.

and a greater damping ratio in the SF. In general, it would weaken the propagation of shear waves. However, the result was the opposite. This is attributed to the soil-structure dynamic interaction.

Fig. 10 compares the acceleration time histories and Arias intensity at A5 in the FF and SF under 0.1 g seismic motions. It is noted that the PGA and the seismic energy in the FF were greater than that in the SF. This indicates that the presence of the underground structure would reduce the acceleration of the soil adjacent to the side walls of the structure.

The comparison of seismic motions at A6 in the FF and SF was presented in Fig. 11 to analyze the effect of the structure on the near-surface ground motion. The results show the difference between the FF and SF. Compared to the SF, there was significant attenuation in the acceleration in the FF. This is because the soil layer at A4 in the FF has completely liquefied and remained in a liquefied state at the end of the shaking (Fig. 7), reflecting the filtering effect of liquefaction on shear waves. However, for the SF, although the r_u reached a high level, it dissipated quickly after reaching its peak, allowing the soil shear stiffness to

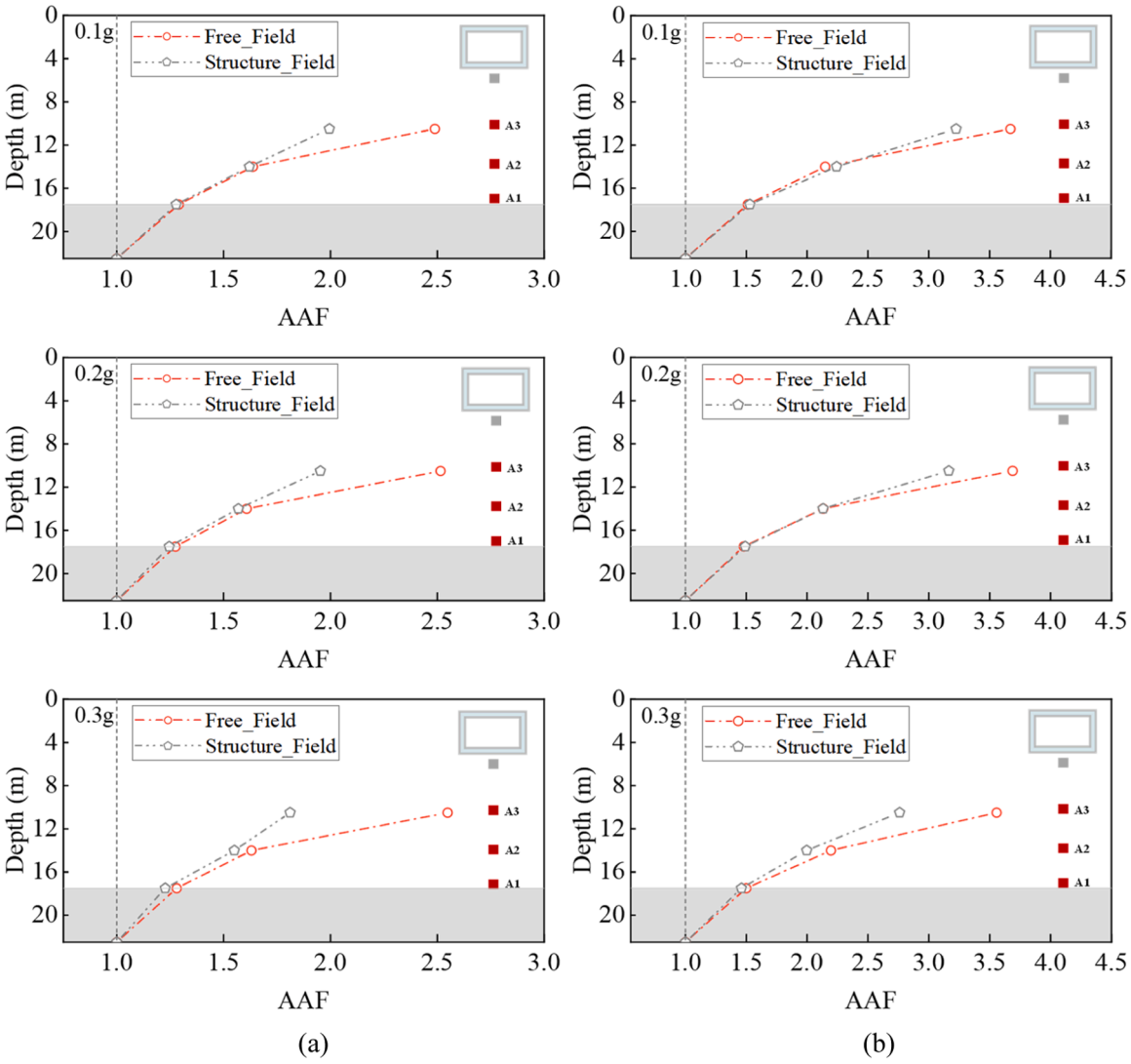

Fig. 8. Arias intensity amplification factor (AAF) beneath the structure (A1-A3) under various motions: (a) Motion1, (b) Motion2.

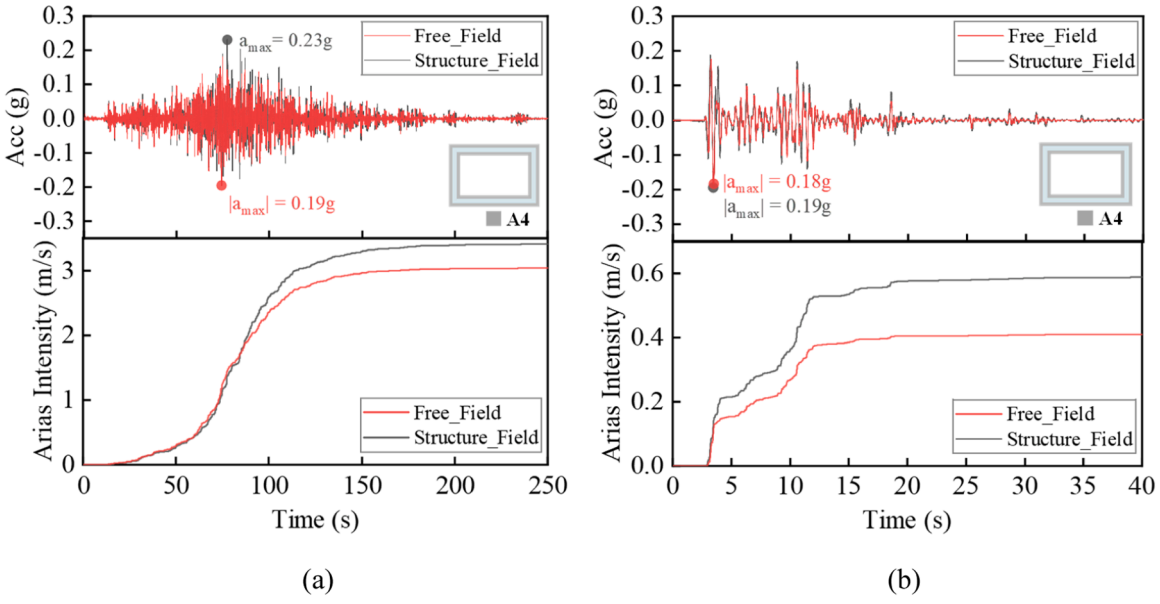

Fig. 9. Acceleration time histories and Arias intensity at A4 under 0.1 g seismic motions: (a) Motion1, (b) Motion2.

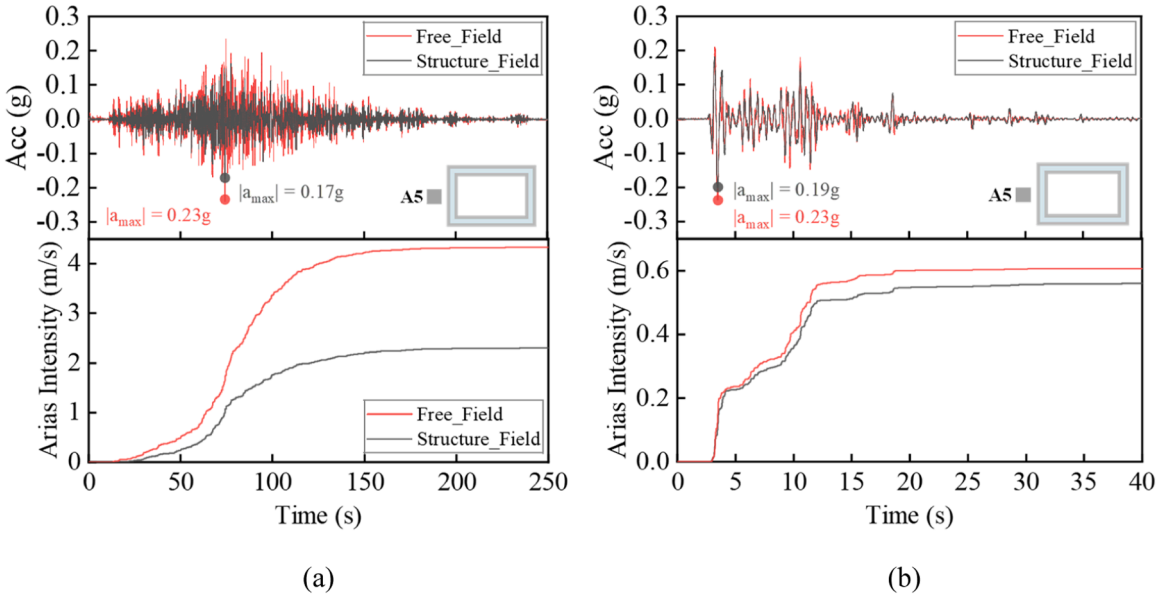

Fig. 10. Acceleration time histories and Arias intensity at A5 under 0.1 g seismic motions: (a) Motion1, (b) Motion2.

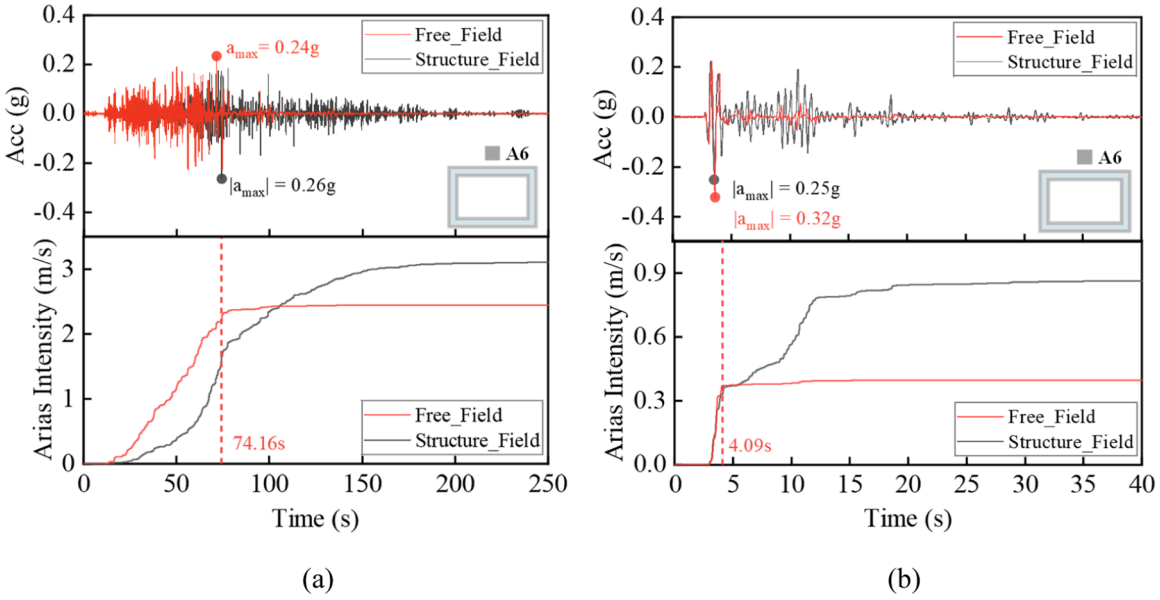

Fig. 11. Acceleration time histories and Arias intensity at A6 under 0.1 g seismic motions: (a) Motion1, (b) Motion2.

recover. This ensured the propagation of shear waves. As shown in Fig. 11(a), the dashed line represents the moment of liquefaction. Both the acceleration and seismic energy in the FF were greater than those in the SF before the soil layer liquefied. But for Moiton2, the seismic energy was close between the two sites before the liquefaction occurred. This is due to the different seismic energy release patterns between Motion1 and Motion2. The PGA at A6 in the SF was larger than that in the FF under the Motion1, while the PGA in the FF was greater under the Motion2. However, the seismic energy in the SF was greater than that in the FF under the two input motions. Thus, for the seismic design of superstructures over underground structures in potentially liquefiable sites, it is inappropriate to use only the PGA as the main parameter for seismic motion design. It is necessary to consider the amplification effect of the underground structure on the seismic energy at the near-surface, as well as the type of seismic motion.

3.2.3. Acceleration response spectra

The influence of the underground structure on acceleration response spectra (ARS) was determined by comparing the acceleration data recorded around the structure between the FF and SF.

For the position near the bottom of the structure, Fig. 12 shows the acceleration response spectra (damping ratio=5%) normalized by PGA at A4 in the FF and SF under different seismic motions. Due to the malfunction of sensor A4 in the SF under 0.2 g Motion1 and 0.3 g Motion2, the corresponding data is not provided in the figure. As shown in Fig. 12(a), amplification of ARS was observed around the period of 0.5 s in the FF under the 0.1 g Motion1, but not in the SF. The results demonstrate that the de-amplification effect of the ARS values near the period of 0.5 s due to the presence of the structure. In addition, a significant attenuation was observed in both the FF and SF within the period range of 0.9–3.0 s, and the curves of these two fields were similar, which indicated that the existence of the structure had no influence on

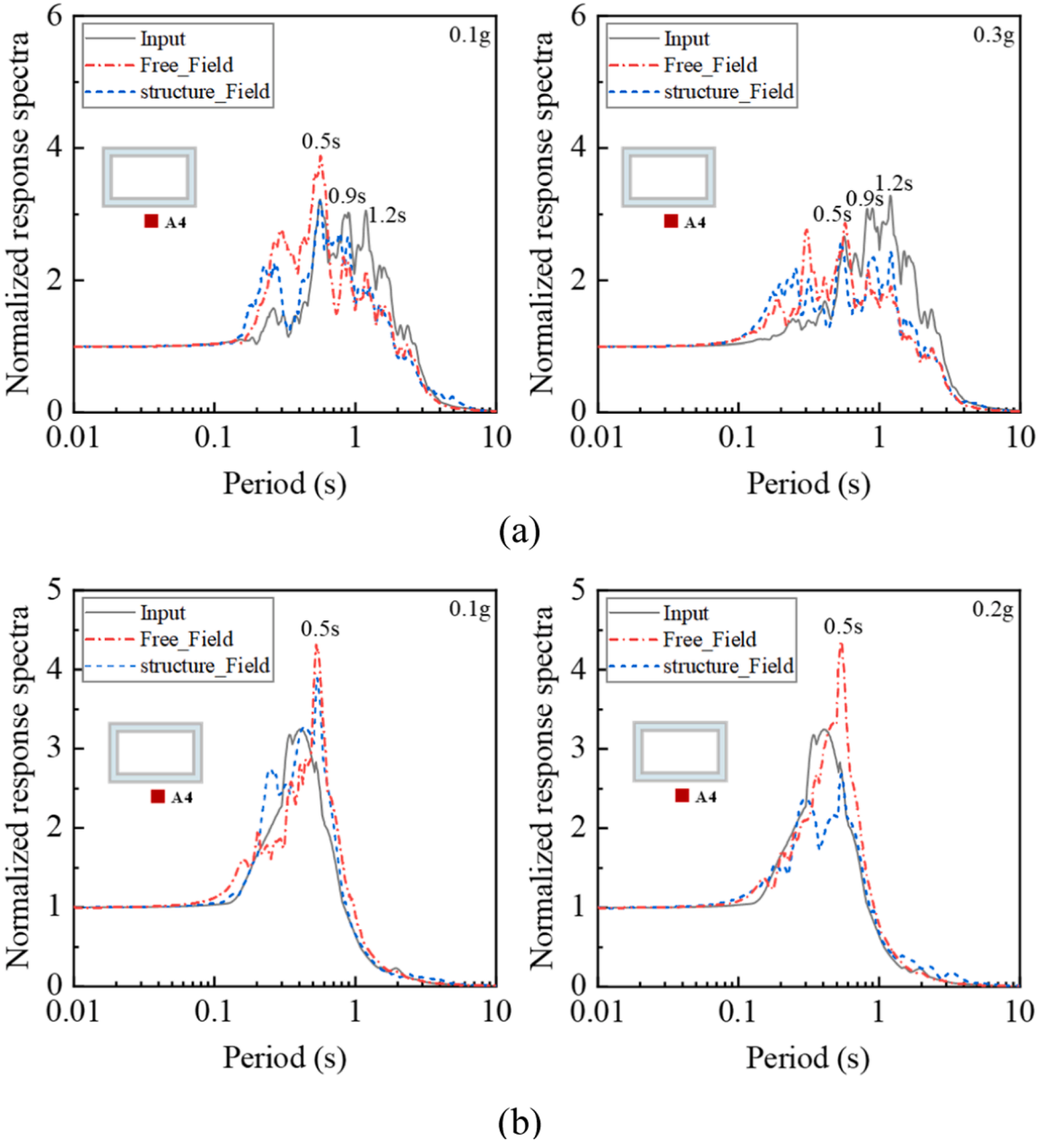

Fig. 12. Normalized response spectra at A4 in the FF and SF under different seismic motions: (a) Motion1, (b) Motion2.

acceleration response within this period range. The de-amplification effect of the structure was also observed under the Motion2, and this effect became more pronounced with the increase in ground motion intensity.

For the position adjacent to the side walls of the structure, Fig. 13 presents the normalized response spectra at A5 in the FF and SF under different seismic motions. As shown in Fig. 13(a), under the 0.1 g Motion1, the amplification around the period of 0.5 s in the SF was greater than that in the FF due to the effect of the structure. This phenomenon was also observed under the 0.1 g Motion2. There was a heavy attenuation within the period range of 0.9–3.0 s in the FF under the Motion1. However, the attenuation of response spectra was weakened due to the existence of the structure in the SF, especially for the period of 0.90–1.2 s. In addition, the effect of the structure reduced with the increase of the amplitude of input motions.

For the position above the structure, Fig. 14 displays the comparison of normalized response spectra at A6 between the FF and SF under different seismic motions. The results in Fig. 14(a) show that the presence of the structure could weaken the attenuation of the ARS values within the period range of 0.9–3.0 s, especially for around the period of 1.2 s. As shown in Fig. 14(b), due to the effect of the structure, the ARS values around the period of 0.5 s in the SF were greater than those in the FF under the Motion2. This was different from the behavior observed under the Motion1. It could be attributed to the different liquefaction processes in the soil layers above the structure. As shown in Fig. 11, for the Motion2, liquefaction occurred in the soil layers at the beginning of the shaking, causing the shear waves to attenuate rapidly. But for the Motion1, a portion of shear wave propagation was maintained before liquefaction happened.

Fig. 15 shows the normalized response spectra of the underground structure and the soil adjacent to the side walls of the structure in the SF under 0.1 g seismic motions. Clearly, the acceleration frequency component distributions of the underground structure exhibited a high similarity to that of the soil adjacent to the structure's side walls,

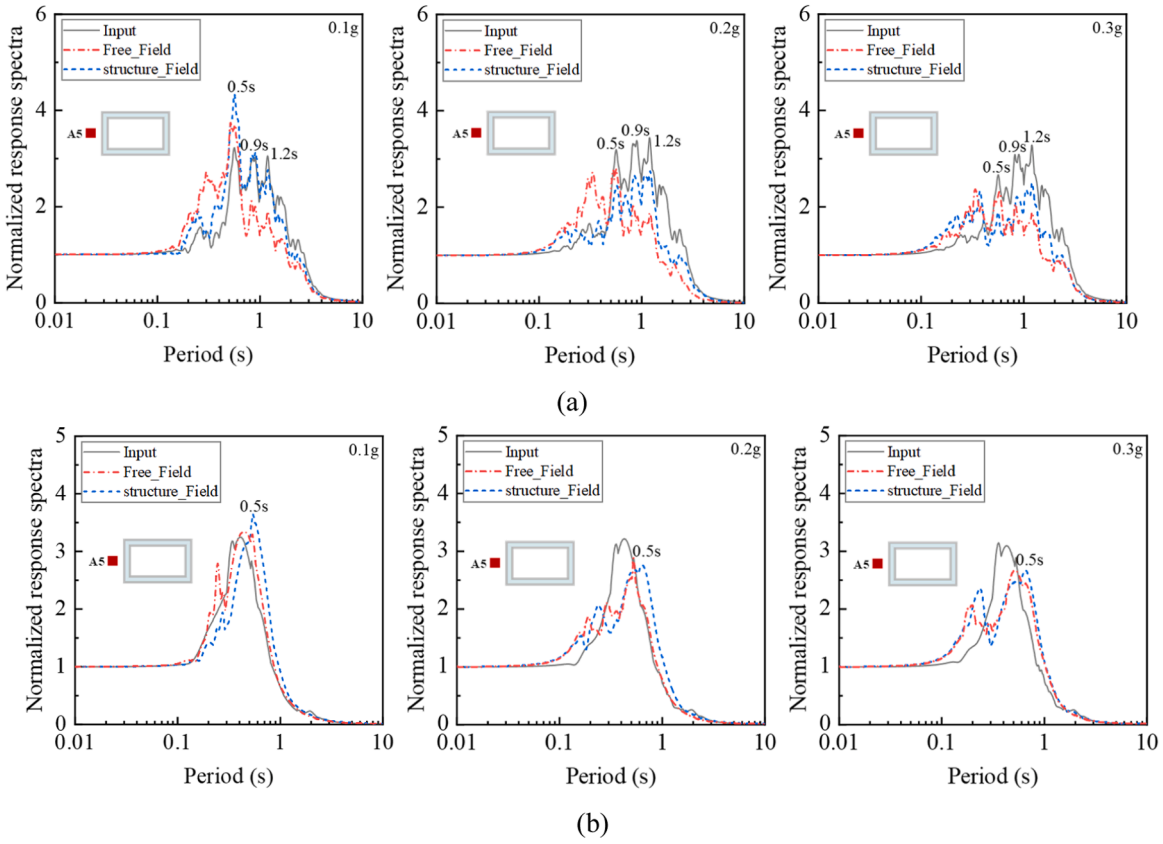

Fig. 13. Normalized response spectra at A5 in the FF and SF under different seismic motions: (a) Motion1, (b) Motion2.

reflecting the dominant role of soil movement in influencing the seismic response of the underground structure. The same results were obtained from a previous study (Zhu et al., 2021).

3.3. Effect of the underground structure on shear stress-strain behavior

To investigate the effect of the structure on the shear stress-strain behavior of the soil adjacent to the side walls of the structure, the shear stress and shear strain at A5 were calculated from acceleration time histories according to the method used in previous studies (Zeghal et al., 1999, 1995). The shear stress at a depth z_i can be obtained by Eq. (3).

$$\tau_i(t) = \tau_{i-1} + \rho_{i-1}\frac{\ddot{u}_{i-1} + \ddot{u}_i}{2}\Delta z_{i-1} \quad (i = 2,\ 3,\ \ldots) \tag{3}$$

In which subscript i refers to level z_i, $\tau_i = \tau(z_i,\ t)$, $\ddot{u}_i = \ddot{u}(z_i,\ t)$, Δz_i is the spacing interval and ρ_{i-1} is the average mass density for the soil layer between levels z_{i-1} and z_i. The shear strain can be calculated by Eq. (4).

$$\gamma_i(t) = \frac{1}{\Delta z_{i-1} + \Delta z_i}\left[(u_{i+1} - u_i)\frac{\Delta z_{i-1}}{\Delta z_i} + (u_i - u_{i-1})\frac{\Delta z_i}{\Delta z_{i-1}}\right](2,\ 3,\ \ldots) \tag{4}$$

Where $u_i = u(z_i,\ t)$ is displacement evaluated through double integration of the corresponding acceleration histories. The shear stress and the shear strain are second-order accurate. Additionally, the Butterworth band-pass filter (0.2–6.0 Hz) was employed to process the acceleration time histories to remove noise and mitigate drift errors during the integration process.

3.3.1. Shear stress and shear strain

Fig. 16 presents the maximum values of shear stress (τ_{max}) at A5 in the FF and SF under different input motions. The τ_{max} in the FF was much smaller compared to the SF data. The results demonstrate the effect of the structure on the shear stress of the soil adjacent to the side walls of the structure. As the PGA of the earthquake at the model base increased, the effect of the underground structure was more pronounced in increasing the τ_{max}. Due to the soil-structure interaction, the shear stress of the soil adjacent to the side walls of the structure was amplified.

The time histories of shear strain at A5 in the FF and SF under the Motion1 are shown in Fig. 17. It is noted from Fig. 17 that the shear strain of the SF was smaller in comparison with the FF. In addition, the difference in maximum shear strain (γ_{max}) between the FF and SF increased with the increasing intensity of ground motion. As shown in Fig. 6, the excess pore pressure at P4 in the SF was larger than that in the FF, indicating a greater degradation of stiffness. However, due to the existence of the underground structure, the soil experienced smaller shear strain under greater shear stress. It could be concluded that the structure limited the deformation of the soil adjacent to its side walls.

3.3.2. Equivalent shear modulus

To investigate the effect of the structure on the shear modulus of the soil adjacent to the side walls of the structure, the approach of Brennan et al. (2005) was applied to compute equivalent shear modulus G_e. It can be obtained by Eq. (7).

$$\tau_c = \frac{\tau_{max} - \tau_{min}}{2} \tag{5}$$

$$\gamma_c = \frac{\gamma_{max} - \gamma_{min}}{2} \tag{6}$$

$$G_e = \frac{\tau_c}{\gamma_c} \tag{7}$$

Where τ_{max} and τ_{min} represent the maximum and minimum values of shear stress during a shear stress-strain loop, respectively. γ_{max} and γ_{min} represent the maximum and minimum values of shear strain developed

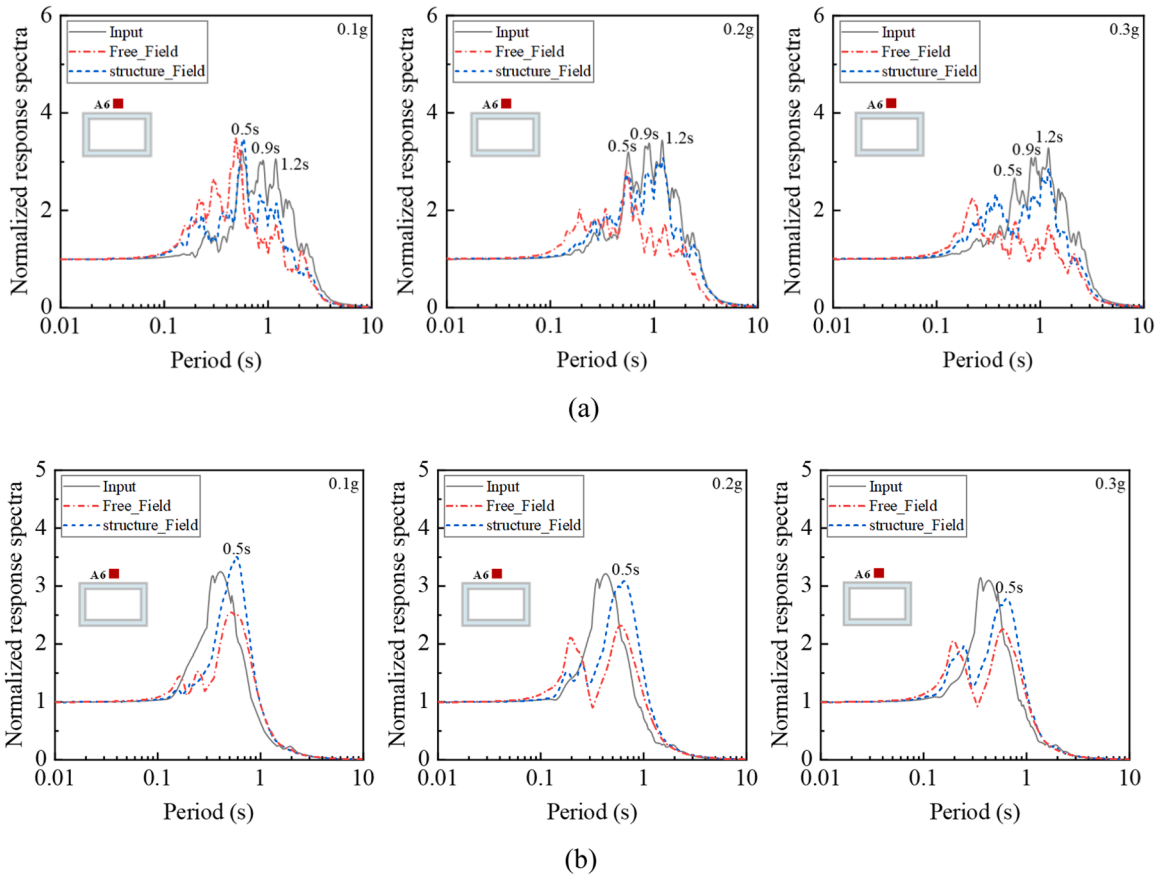

Fig. 14. Normalized response spectra at A6 in the FF and SF under different seismic motions: (a) Motion1, (b) Motion2.

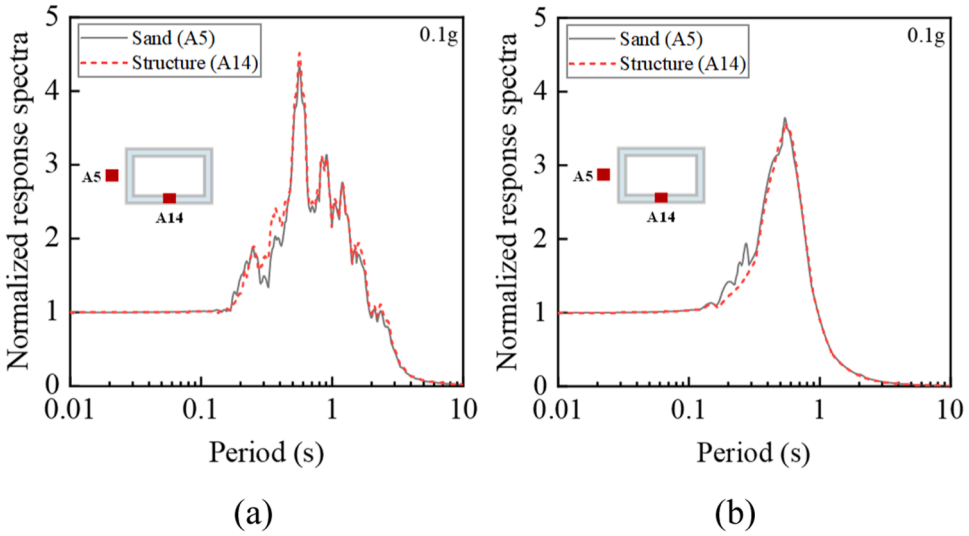

Fig. 15. Normalized response spectra of the underground structure and the soil adjacent to side walls of the structure in the SF under 0.1 g seismic motions: (a) Motion1, (b) Motion2.

in the loop, respectively.

The first shear stress-strain loop of Motion2 was selected to explore the effect of the underground structure on shear modulus. Fig. 18 shows the time histories of shear strain and selected shear stress-strain loops at A5 in the FF and SF under the Motion2. It is noted from Fig. 18 that the G_e at A5 was larger in the SF than that in the FF under the same shaking, signifying that the soil-structure dynamic interaction increased the shear modulus of the soil adjacent to the side walls of the structure. Furthermore, for the selected shear stress-strain loops, the difference in the G_e value between the FF and SF increased as the PGA of the seismic motion increased. It indicated that the effect of the underground structure became more pronounced with the increase in the input motion intensity.

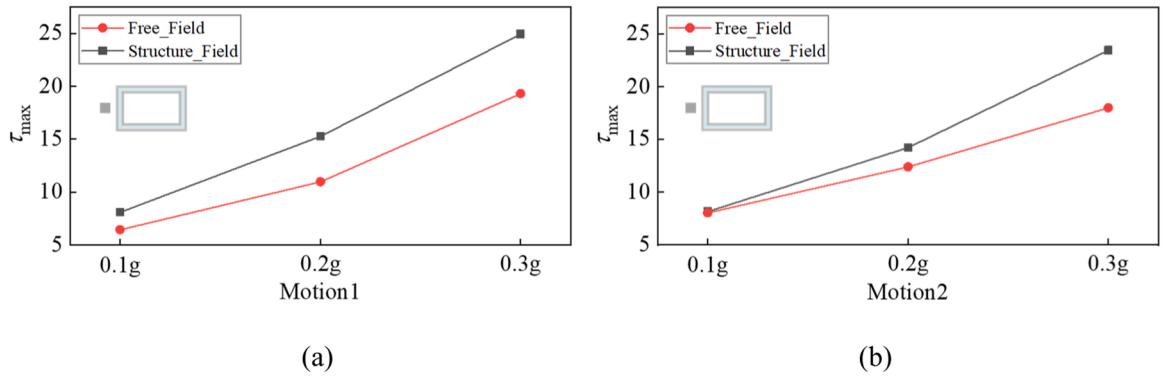

Fig. 16. Maximum values of shear stress (τ_{max}) at A5 in the FF and SF under different intensities of seismic motions: (a) Motion1, (b) Motion2.

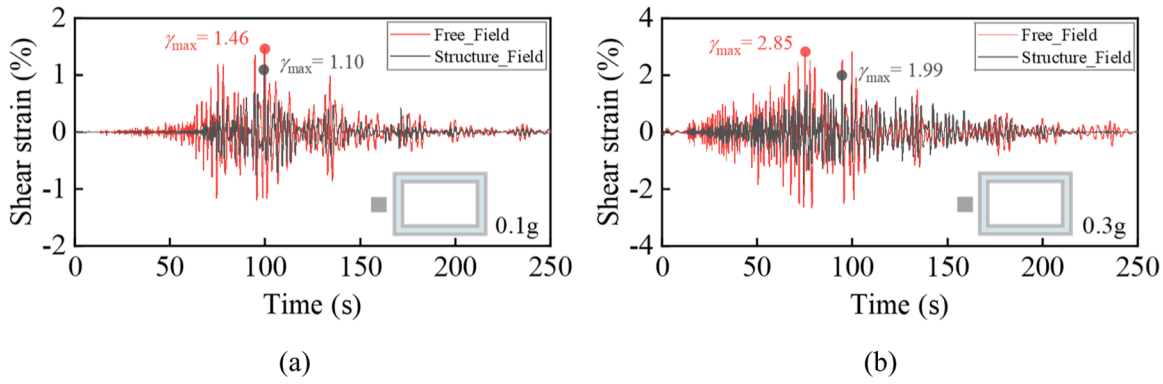

Fig. 17. The time histories of shear strain at A5 in the FF and SF under the Motion1: (a) 0.1 g, (b) 0.3 g.

4. Conclusions

In this study, 50 g centrifuge shaking table tests were conducted to investigate the effect of an underground structure on the seismic responses of saturated coral sand sites. By comparing the experimental results of the free field and structure field, the differences in pore pressure response, acceleration response, and shear stress-strain behavior between the two sites were discussed and analyzed. The main conclusions are as follows:

(1) Compared to the free field, the underground structure increased the liquefaction depth of the soil beneath it. Additionally, the presence of the structure led to an increase in the excess pore pressure in the soil near the side walls and the bottom of the structure, while causing a decrease in the excess pore pressure in the soil layers above the structure. Due to the structure blocking the continuing upward migration of pore fluid from the deep to the shallow layer, the excess pore pressure in the soil layer above the structure dissipated rapidly after reaching its peak and had completely dissipated by the end of the shaking. Furthermore, soil-underground structure dynamic interaction resulted in higher dilatancy in the soil layers near the bottom of the structure.

(2) For the soil layers beneath the underground structure, the influence of the structure on seismic wave propagation gradually decreased with increasing distance from the structure. The underground structure was observed to influence the acceleration response of the surrounding soil. Compared to the free field, soil-structure interaction amplified the seismic motions in the soil layers near the bottom of the structure, whereas it reduced the seismic energy in the soil layers adjacent to the structure's side walls. For the soil above the structure, significant attenuation in the acceleration was observed in the FF due to soil liquefaction, which caused the seismic energy in the SF to be greater than that in the FF under the same shaking. It can be concluded that the underground structure had an amplification effect on the seismic motions in the soil above the structure. However, this behavior cannot be fully reflected by the PGA values of the soil layers.

(3) The structure has a significant influence on the acceleration response spectra of the surrounding soil. For the position near the bottom of the structure, the de-amplification effect of the structure in the ARS values was observed near the period of 0.5 s. The structure had no influence on acceleration response within the period of 0.90–1.2 s. For the soil near the sidewalls and above the structure, the presence of the structure weakened the attenuation of the ARS values within the period range of 0.9–3.0 s.

(4) For the soil near the side walls of the structure, the underground structure amplified the maximum values of shear stress, and the effect of the underground structure was more pronounced with the increase of seismic intensity. In addition, the presence of the structure reduced the deformation of the soil and increased the soil shear modulus.

CRediT authorship contribution statement

Zhongxiang Zhang: Writing – original draft, Visualization, Validation, Investigation, Formal analysis. **Su Chen:** Writing – review & editing, Methodology, Investigation, Conceptualization. **Yongzhi Wang:** Writing – review & editing, Resources, Data curation. **Xiaojun Li:** Writing – review & editing, Supervision, Resources.

Declaration of competing interest

The authors declared that they have no conflicts of interest to this

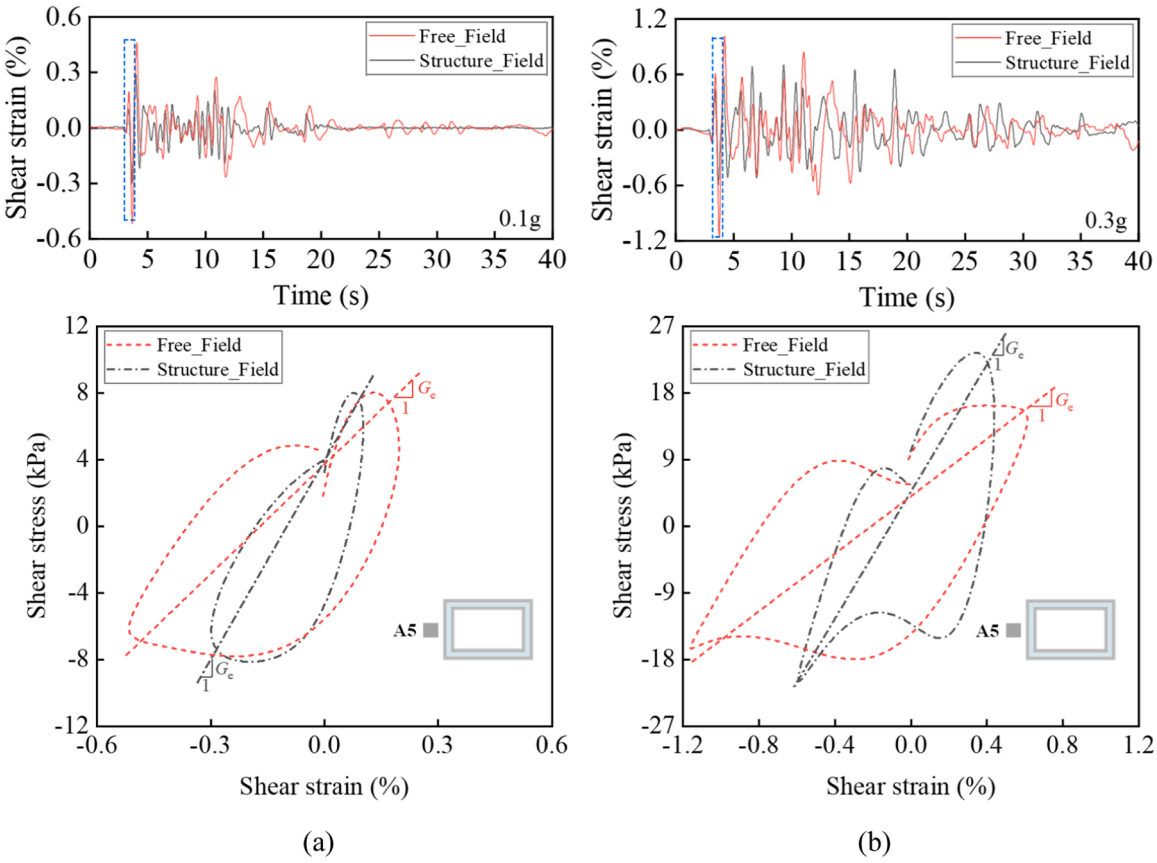

Fig. 18. The time histories of shear strain and selected shear stress-strain loops at A5 in the FF and SF under the Motion2: (a) 0.1 g, (b) 0.3 g.

work. We declare that we do not have any commercial or associative interest that represents a conflict of interest in connection with the work submitted.

Acknowledgments

This work is under the support of the National Natural Science Foundation of China (Grant Numbers 51878626 and 52192675).

References

Abuhajar, O., El Naggar, H., Newson, T., 2015. Experimental and numerical investigations of the effect of buried box culverts on earthquake excitation. Soil Dyn. Earthq. Eng. 79, 130–148. https://doi.org/10.1016/j.soildyn.2015.07.015.

Adamidis, O., Madabhushi, G.S.P., 2015. Use of viscous pore fluids in dynamic centrifuge modelling. Int. J. Phys. Model. Geotech. 15, 141–149. https://doi.org/10.1680/jphmg.14.00022.

Arias, A., 1970. A Measure of Earthquake Intensity. MIT Press, pp. 438–483.

Baziar, M.H., Moghadam, M.R., Kim, D.-S., Choo, Y.W., 2014. Effect of underground tunnel on the ground surface acceleration. Tunn. Undergr. Space Technol. 44, 10–22.

Besharat, V., Davoodi, M., Jafari, M.K., 2012. Effect of underground structures on free-field ground motion during earthquakes. In: 15th World Conference on Earthquake Engineering.

Brennan, A.J., Thusyanthan, N.I., Madabhushi, S.P., 2005. Evaluation of Shear Modulus and Damping in Dynamic Centrifuge Tests. J. Geotech. Geoenvironmental Eng. 131, 1488–1497.

Chen, G., Qin, Y., Ma, W., Liang, K., Wu, Q., Juang, C.H., 2024. Liquefaction susceptibility and deformation characteristics of saturated coral sandy soils subjected to cyclic loadings – a critical review. Earthq. Eng. Eng. Vib. 23, 261–296. https://doi.org/10.1007/s11803-024-2221-4.

Chock, G., Kindred, T., Robertson, I., Iinuma, G., Nicholson, P., Lau, E., Brandes, H., Sarwar, A., Medley, E., Pino, J., Okubo, P., Holmes, W., Hirshorn, B., Sumada, J., 2006. Compilation of Observations of the October 15, 2006 Kiholo Bay (Mw 6. 7) and Mahukona (Mw 6.0) Earthquakes. Hawai'i.

Ding, X., Zhang, Y., Wu, Q., Chen, Z., Wang, C., 2021. Shaking table tests on the seismic responses of underground structures in coral sand. Tunn. Undergr. Space Technol. 109, 103775.

Ding, Z., He, S.-H., Sun, Y., Xia, T.-D., Zhang, Q.-F., 2021. Comparative study on cyclic behavior of marine calcareous sand and terrigenous siliceous sand for transportation infrastructure applications. Constr. Build. Mater. 283, 122740. https://doi.org/10.1016/j.conbuildmat.2021.122740.

Dou, P., Xu, C., Du, X., Chen, S., 2022. Influence of structure on the aseismic stability and dynamic responses of liquefiable soil. Bull. Earthq. Eng. 20, 55–76.

Feizi, D., Asgari Marnani, J., Alielahi, H., Panji, M., 2022. Seismic ground amplification induced by box-shaped tunnels. Earthq. Eng. Eng. Vib. 21, 697–714.

Gao, R., Ye, J., 2023. Mechanical behaviors of coral sand and relationship between particle breakage and plastic work. Eng. Geol 316, 107063. https://doi.org/10.1016/j.enggeo.2023.107063.

Ha Giang, P.H., Van Impe, P.O., Van Impe, W.F., Menge, P., Haegeman, W., 2017. Small-strain shear modulus of calcareous sand and its dependence on particle characteristics and gradation. Soil Dyn. Earthq. Eng. 100, 371–379. https://doi.org/10.1016/j.soildyn.2017.06.016.

Hughes, F., Madabhushi, S., 2018. The importance of vertical accelerations in liquefied soils. In: Physical Modelling in Geotechnics, 2. CRC Press, pp. 967–973. Volumepp.

Isari, M., Razavi, S.K., Tarinejad, R., Sobhkhiz Foumani, R., 2022. Investigating the Effects of Underground Structures on the Scattering of Seismic Waves Reaching the Ground Surface. Transp. Infrastruct. Geotechnol. 9, 321–337. https://doi.org/10.1007/s40515-021-00177-4.

Jafarian, Y., Fallahzedeh, M., Lee, C.-J., Haddad, A., Hedayati, J., 2021. Centrifuge Modeling for Seismic Performance of Floating Piled Raft with and without Drainage Wells in Liquefiable Site. Int. J. Geomech. 21, 04021046. https://doi.org/10.1061/(ASCE)GM.1943-5622.0001994.

Javdanian, H., Jafarian, Y., 2018. Dynamic shear stiffness and damping ratio of marine calcareous and siliceous sands. Geo-Mar. Lett. 38, 315–322. https://doi.org/10.1007/s00367-018-0535-9.

Kutter, B.L., 1992. Dynamic centrifuge modeling of geotechnical structures. Transp. Res. Rec.

Kutter, B.L., Carey, T.J., Stone, N., Zheng, B.L., Gavras, A., Manzari, M.T., Zeghal, M., Abdoun, T., Korre, E., Escoffier, S., 2020. LEAP-UCD-2017 Comparison of Centrifuge Test results, in: Model Tests and Numerical Simulations of Liquefaction and Lateral Spreading: LEAP-UCD-2017. Springer, pp. 69–103.

Liu, L., Yao, X., Ji, Z., Gao, H., Wang, Z., Shen, Z., 2021. Cyclic Behavior of Calcareous Sand from the South China Sea. J. Mar. Sci. Eng. 9, 1014. https://doi.org/10.3390/jmse9091014.

Liu, X., Li, S., Sun, L., 2020. The study of dynamic properties of carbonate sand through a laboratory database. Bull. Eng. Geol. Environ. 79, 3843–3855. https://doi.org/10.1007/s10064-020-01785-z.

Ma, W., Qin, Y., Zhao, K., Chen, G., 2021. Comparisons on liquefaction behavior of saturated coral sand and quartz sand under principal stress rotation. Mar. Georesources Geotechnol. 1–13.

Manandhar, S., Kim, S.-N., Ha, J.-G., Ko, K.-W., Lee, M.-G., Kim, D.-S., 2021. Liquefaction evaluation using frequency characteristics of acceleration records in KAIST centrifuge tests for LEAP. Soil Dyn. Earthq. Eng. 140, 106332. https://doi.org/10.1016/j.soildyn.2020.106332.

Mashhadban, H., Choobbasti, A.J., Shooshpasha, I., Ashtiani, M., 2021. Evaluation of the seismic response of the slopes in the presence of the horseshoe tunnel. Bull. Eng. Geol. Environ. 80, 157–177. https://doi.org/10.1007/s10064-020-01920-w.

Mejia, Yeung, 1995. Liquefaction of Coralline Soils During the 1993 Guam earthquake. San Diego, USA.

Olson, S.M., Green, R.A., Lasley, S., Martin, N., Cox, B.R., Rathje, E., Bachhuber, J., French, J., 2011. Documenting Liquefaction and Lateral Spreading Triggered by the 12 January 2010 Haiti Earthquake. Earthq. Spectra 27, 93–116. https://doi.org/10.1193/1.3639270.

Rabeti Moghadam, M., Baziar, M.H., 2016. Seismic ground motion amplification pattern induced by a subway tunnel: shaking table testing and numerical simulation. Soil Dyn. Earthq. Eng. 83, 81–97. https://doi.org/10.1016/j.soildyn.2016.01.002.

Sun, Q., Dias, D., Guo, X., Li, P., 2019. Numerical study on the effect of a subway station on the surface ground motion. Comput. Geotech. 111, 243–254. https://doi.org/10.1016/j.compgeo.2019.03.026.

Tsinidis, G., Heron, C., Pitilakis, K., Madabhushi, G., 2014. Physical modeling for the evaluation of the seismic behavior of square tunnels. Seism. Eval. Rehabil. Struct. 389–406.

Wang, G., Yuan, M., Miao, Y., Wu, J., Wang, Y., 2018. Experimental study on seismic response of underground tunnel-soil-surface structure interaction system. Tunn. Undergr. Space Technol. 76, 145–159. https://doi.org/10.1016/j.tust.2018.03.015.

Wang, J., Yang, J., Zhuang, H., Ma, G., Sun, Y., 2022. Seismic Responses of a Large Unequal-span Underground Subway Station in Liquefiable Soil Using Shaking Table Test. J. Earthq. Eng. 26, 8446–8467. https://doi.org/10.1080/13632469.2021.1991523.

Wang, R., Zhu, T., Yu, J.-K., Zhang, J.-M., 2022. Influence of vertical ground motion on the seismic response of underground structures and underground-aboveground structure systems in liquefiable ground. Tunn. Undergr. Space Technol. 122, 104351. https://doi.org/10.1016/j.tust.2021.104351.

Wang, X., Ding, H., Meng, Q., Wei, H., Wu, Y., Zhang, Y., 2021. Engineering characteristics of coral reef and site assessment of hydraulic reclamation in the South China Sea. Constr. Build. Mater. 300, 124263. https://doi.org/10.1016/j.conbuildmat.2021.124263.

Wu, Q., Ding, X., Zhang, Y., 2023a. Dynamic interaction of coral sand-pile-superstructure during earthquakes: 3D numerical simulations. Mar. Georesources Geotechnol. 41, 774–790.

Wu, Q., Ding, X., Zhang, Y., Chen, Z., 2020. Comparative study on seismic response of pile group foundation in coral sand and fujian sand. J. Mar. Sci. Eng. 8, 189.

Wu, Q., Ding, X., Zhang, Y., Xin, Y., 2024. Experimental and numerical study on dynamic response of underground structure in coral sand under earthquakes. J. Earthq. Eng. 28, 62–84. https://doi.org/10.1080/13632469.2023.2173491.

Wu, Q., Ding, X., Zhang, Yanling, Zhang, Yanli, 2023b. Numerical analysis of seismic response of rectangular underground structure in coral sand. Undergr. Space 9, 155–172.

Wu, Q., Liu, Q., Zhuang, H., Chen, G., Du, X., 2023. Liquefaction characteristics of saturated marine coral sand with different non-plastic fines content subjected to complex cyclic stress paths. Ocean Eng. 281, 114794. https://doi.org/10.1016/j.oceaneng.2023.114794.

Xiao, Y., Liu, H., Chen, Q., Ma, Q., Xiang, Y., Zheng, Y., 2017. Particle breakage and deformation of carbonate sands with wide range of densities during compression loading process. Acta Geotech. 12, 1177–1184. https://doi.org/10.1007/s11440-017-0580-y.

Xinzhi, Wang, 2008. Study On Engineering Geological Properties of Coral reefs and Feasibility of Large Project Construction on Nansha Islands (PhD thesis). Institute of Rock and Soil Mechnics. The Chinese Academy of Sciences, Wuhan, China.

Yatsumoto, H., Mitsuyoshi, Y., Sawamura, Y., Kimura, M., 2019. Evaluation of seismic behavior of box culvert buried in the ground through centrifuge model tests and numerical analysis. Undergr. Space 4, 147–167. https://doi.org/10.1016/j.undsp.2018.09.007.

Zeghal, M., Elgamal, A.-W., Tang, H.T., Stepp, J.C., 1995. Lotung downhole array. II: evaluation of soil nonlinear properties. J. Geotech. Eng. 121, 363–378. https://doi.org/10.1061/(ASCE)0733-9410(1995)121:4(363).

Zeghal, M., Elgamal, A.-W., Zeng, X., Arulmoli, K., 1999. Mechanism of liquefaction response in sand–silt dynamic centrifuge tests. Soil Dyn. Earthq. Eng. 18, 71–85.

Zhang, H., Liang, F., Chen, H., 2021. Seismic response of offshore composite caisson-piles foundation with different pile configurations and soil conditions in centrifuge tests. Ocean Eng. 221, 108561. https://doi.org/10.1016/j.oceaneng.2020.108561.

Zhang, Z., Chen, S., Li, X., Wang, Y., Long, H., 2024. Centrifuge modeling of seismic response of saturated coral sand with wide gradation under offshore ground motions. Soil Dyn. Earthq. Eng. 185, 108877. https://doi.org/10.1016/j.soildyn.2024.108877.

Zhu, T., Hu, J., Zhang, Z., Zhang, J.-M., Wang, R., 2021. Centrifuge Shaking Table Tests on Precast Underground Structure–Superstructure System in Liquefiable Ground. J. Geotech. Geoenvironmental Eng. 147, 04021055. https://doi.org/10.1061/(ASCE)GT.1943-5606.0002549.